JM PAPERS

Excitation and evolution of radiating modes in supersonic boundary layers. Part 2. Back effect of spontaneously radiated Mach waves

Fufeng Qin[1] **and Xuesong Wu**[1],†

[1]Department of Mathematics, Imperial College London, 180 Queen's Gate, London SW7 2AZ, UK

This paper investigates the linear and nonlinear evolution of radiating modes under the influence of the spontaneously emitted Mach waves in a simple set-up of the supersonic boundary layers that develop in the entry region of a channel formed by two parallel semi-infinite flat plates. Two scenarios are considered. The first occurs in the boundary layers having identical wall conditions, where the Mach wave emitted by a radiating mode in one boundary layer influences the instability in the other. The second scenario takes place when the wall temperatures are different, in which case the spontaneously radiated Mach wave is reflected by the other boundary layer back to act on the radiating mode. Appropriate amplitude equations with the acoustic feedback effect being accounted for are derived. In each case, the effect of the spontaneously emitted sound contributes a linear term of delay type to the respective amplitude equation. For the first scenario, analytical and numerical studies of the amplitude equations show that due to the back action of the spontaneously radiated Mach wave, the amplitude exhibits rapid oscillations, and in the case of enhanced feedback effects, its envelope experiences near extinction followed by resurrection. The study of the coupled equations shows that the two modes with different initial amplitudes either undergo oscillations before attenuating, or terminate a finite-distance singularity at different locations. For the second scenario, the acoustic feedback produces similar effects in a broad range of wall temperature. The effects become pronounced, and the dependence on the wall temperature becomes more sensitive when the latter approaches the value corresponding to the resonance. Estimates suggest that such acoustic feedback is likely to be present in typical wind tunnel experiments and models for scramjet combustors.

Key words: boundary layer receptivity, boundary layer stability, transition to turbulence

† Email address for correspondence: x.wu@ic.ac.uk

1. Introduction

As discussed in Part 1 (Qin & Wu 2024), acoustic waves impinging on a supersonic boundary layer play an important role in laminar–turbulent transition. On the one hand, as one of the elementary forms of free-stream fluctuations, acoustic waves may excite, and furthermore interact with, the intrinsic instability modes. On the other hand, instability modes may radiate sound waves, which may affect the original source so that an acoustic feedback loop forms; this scenario will be examined in the present study.

Acoustic feedback can take place in many situations, and may be categorised broadly into two types. The first involves coupling between the regions in the streamwise direction. One typical case is associated with a shear layer encountering abrupt changes. An important example is the laminar flow past an aerofoil, where the instability modes developing in the boundary layer over the aerofoil surface are scattered by the strong local inhomogeneity near the trailing edge to radiate sound waves, which propagate upstream and regenerate the instability mode, thereby forming a self-sustained feedback loop. As a result, tonal noise is produced, whose spectrum features strong peaks at discrete frequencies. It has been observed experimentally (Paterson *et al.* 1973; Arbey & Bataille 1983) that the dominant frequency of the feedback tone undergoes sudden switches when the relevant parameters are gradually varied, a phenomenon referred to as a 'ladder-structure'. The global feedback loop with discrete tonal frequencies has also been confirmed by high-fidelity numerical simulations (Desquesnes, Terracol & Sagaut 2007; Jones, Sandberg & Sandham 2010; Jones & Sandberg 2011). Back action of sound and the flow–acoustic coupling of this type were reviewed by Rockwell & Naudasher (1979) and Golubev (2021). A complete mathematical model or description for tonal noise does not exist. In order to mimic the essential physics, the acoustic feedback was considered in a simpler setting (Wu 2011), a subsonic boundary-layer flow over a nominally flat plate, on which two well-separated localised roughness elements are present. In this case, the global acoustic feedback loop is established by an instability wave amplifying and being scattered by the downstream roughness to radiate sound waves, which in turn propagate upstream and interact with the upstream roughness to regenerate the instability wave. The closed-loop interaction leads to a global absolute instability, which features self-sustained oscillations as well as pronounced noise emission at discrete frequencies (Wu 2011, 2014). The main theoretical predictions were supported by experiments (Abo, Inasawa & Asai 2021).

In addition to the acoustic feedback loop developing in the streamwise direction, transverse acoustic coupling may occur if the flow is confined in a finite domain. For example, transverse acoustic coupling may take place in conventional wind tunnel experiments, where the test model is exposed to a significant amount of noise either generated or reflected by the turbulent boundary layer on the nozzle wall (Laufer 1961; Schneider 2001; Graziosi & Brown 2002). The effects are particularly significant and problematic in the supersonic regime as a supersonic turbulent boundary layer emits strong noise (mostly in the form of Mach waves). Another relevant setting is the duct or combustion chamber of a scramjet, which may be modelled simply as a channel between two well-separated semi-infinite parallel flat plates (e.g. Curran, Heiser & Pratt 1996; Seleznev, Surzhikov & Shang 2019). In the entry region, a developing boundary layer is formed along each plate. Due to the presence of shock waves, a multitude of instabilities may exist in both boundary layers developing on the plates. Transverse acoustic feedback may be established through two-way coupling between radiated sound and instability waves. As a first step to model such coupling, Wu (2014) investigated the instability of the supersonic 'twin boundary layers' developing in the entry region along two semi-infinite

parallel plates. He focused on the instability modes whose characteristic wavelength and frequency comply with the unsteady triple-deck structure. Accordingly, the distance separating the two plates is assumed to be such that the instability modes in the upper and lower boundary layers share a common upper deck. Owing to transverse acoustic feedback, there arises a new spectrum of unstable planar modes, which is absent without the transverse coupling (cf. Smith 1989). The instability of such an entry flow in the incompressible regime had been considered in an earlier study (Smith & Bodonyi 1980), which showed that the presence of a boundary layer modified the Tollmien–Schlichting (T-S) instability.

Effective transverse acoustic coupling may take place between two planar or circular jets, i.e. twin jet configuration (Alkislar *et al.* 2005; Raman, Panickar & Chelliah 2012), or between a jet and a boundary layer developing on a flat plate. The latter scenario can be viewed as modelling the so-called installation effects on the jet noise of an aero-engine installed on the wing (Bushell 1975; Way & Turner 1980). The sound waves emitted from the engine exhaust may be reflected back by the boundary layer developing on a wing surface to impinge on the jet, thereby forming a closed loop. Depending on its distance to the jet, the boundary layer either interacts with the jet aerodynamically or acts merely as a pure reflector. As a consequence, the presence of the boundary layer can substantially affect the radiation property with or without altering the acoustic source. Various prediction models for installation effects have been proposed to study the altered jet noise characteristics (Bhat & Blackner 1998; Moore 2004), which was attributed primarily to scattering of the instability wavepackets in the subsonic regime (Cavalieri *et al.* 2014; Lyu, Dowling & Naqvi 2017; Lyu & Dowling 2018), but in the supersonic regime, acoustic feedback may be established to cause potentially more profound changes to the radiation property. A similar acoustic coupling could be responsible for aeroacoustic and aerodynamic features of twin jets separated by fairly large distances (Bozak & Henderson 2011; Kuo, Cluts & Samimy 2017).

The present paper considers coupling of double supersonic boundary layers through spontaneously radiated Mach waves. Our concern is with the supersonic modes whose characteristic wavelength is comparable to the boundary-layer thickness. As was shown in Wu (2005), these modes radiate highly directional Mach waves, while they are also highly sensitive to incident sound waves with the same frequency and streamwise wavenumber, as was demonstrated in Part 1 of this study. When the two plates are in the same thermal condition, the Mach wave emitted from one of the boundary layers can affect the instability mode of the other, leading to a closed-loop interaction. When the two plates are in similar but not identical conditions, the Mach wave radiated from one boundary layer may be reflected back by the other to influence the development of the radiating mode. These scenarios will be investigated analytically.

The rest of the paper is organised as follows. In § 2, the problem is formulated. We specify the distance between the two plates such that the sound radiation can be described using the near-field formula derived in Part 1. By examining existing experimental data, we show that our formulation is of possibly practical relevance to typical wind tunnel experiments and models for the combustion chamber of a scramjet. Two important cases are presented subsequently. The first is associated with the 'twin boundary layers' developing along two parallel plates in the same thermal state. This is investigated in § 3. As the two identical radiating modes propagating in the upper and lower boundary layers acquire the maximum amplitude, they emit Mach waves spontaneously, and the sound radiated by the upper/lower boundary layer impinges upon the lower/upper boundary layer, forming a coupled system. The amplitude equations accounting for the acoustic coupling are derived, and effects of the distance between the two plates on the modal evolution are

evaluated. In §4, we consider the second case, which is dubbed 'cousin boundary layers'. These boundary layers develop on the plates at different temperatures. The upper boundary layer acts as a reflector when there is a radiating mode only in the lower boundary layer. Effects of the wall temperature on the evolution of the instability waves are studied. Finally, the results are summarised and discussed in §5.

2. Formulation

We consider a supersonic flow in the entry region of a channel between two parallel semi-infinite flat plates separated by a distance h^*. The plates are assumed to be well separated so that there is a uniform core in the bulk while a boundary layer develops along each plate. Such entry flows are of interest in the incompressible, transonic and supersonic regimes; see Smith & Bodonyi (1980), Kluwick & Kornfeld (2014) and references therein for discussions. The flow in the core has mean velocity U_∞, density ρ_∞ and shear viscosity μ_∞. For non-dimensionalisation, U_∞ and a local boundary-layer thickness δ^* are used as the characteristic velocity and length scale, respectively. The dimensionless distance between the two plates is thus $h = h^*/\delta^* \gg 1$. The normalised coordinates (x, y) and time t, as well as the flow quantities (ρ, u, v, p, θ), are the same as those introduced in Part 1. The Reynolds number R and Mach number M remain as

$$R = \rho_\infty U_\infty \delta^*/\mu_\infty, \quad M = U_\infty/a_\infty, \quad (2.1a,b)$$

where a_∞ denotes the sound speed. We focus on two important configurations, namely the 'twin boundary layers' and 'cousin boundary layers', which arise respectively when the plates are at the same or different temperatures.

We are interested in the case where the non-dimensional distance h is of $O(R^{1/2})$ so that the sound radiation can be described using the near-field formula given by (6.9) in Part 1, hence we introduce the rescaled distance $\bar{h}$ by writing

$$h = R^{1/2}\bar{h}. \quad (2.2)$$

Note that the separation of the two plates is much greater than those in the set-ups considered by Wu (2014), Smith & Bodonyi (1980) and Kluwick & Kornfeld (2014). The flow over the lower wall is described by the Cartesian coordinate system (x, y^-), where x is along the plate, and $y^- \equiv y$ is normal to the plate. Furthermore, we introduce $\bar{y}^- \equiv \bar{y} = R^{-1/2}y$ to describe the Mach wave field, hence the upper plate position corresponds to $\bar{y}^- = \bar{h}$. Similarly, the flow beneath the upper plate is described using (x, y^+) with $y^+ = h - y^-$, and the lower plate is at $\bar{y}^+ \equiv \bar{h} - \bar{y}^- = \bar{h}$. A sketch of the double boundary layers is shown in figure 1. Hereafter, the signs '$+/-$' refer to the upper/lower wall, respectively, and the notations introduced in Part 1 will be retained.

2.1. *Practical relevance of the model*

Before specifying the problem, let us first show the practical relevance of our model that uses the near-field formula of the sound radiation. The displacement thickness δ_d^* is related to the boundary-layer thickness δ^* by

$$\delta_d^*/\delta^* = \int_0^\infty (1 - \bar{R}\bar{U})\,\mathrm{d}y = \int_0^\infty (\bar{T} - \bar{U})\,\mathrm{d}\eta, \quad (2.3)$$

where $\bar{R}$, $\bar{U}$ and $\bar{T}$ are the base-flow density, velocity and temperature respectively, given by (2.6) and (2.8) in Part 1. As was shown in Part 1, a radiating mode exists in a
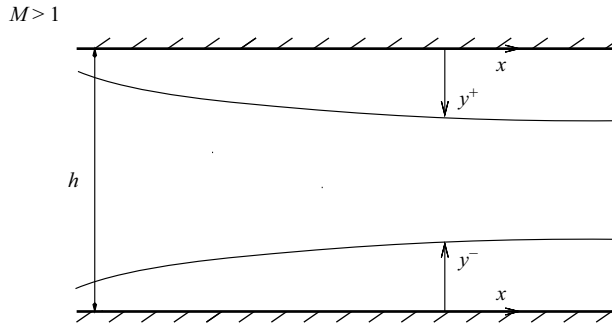
985 A14-4

Figure 1. A sketch of the double boundary layers.

$M = 6$ boundary layer with a $\bar{T}_w = 3$ isothermal surface. Using this base-flow condition, the displacement thickness is found to be

$$\delta_d^* = 8.047\delta^*. \tag{2.4}$$

Typical unit Reynolds numbers R_{unit} are in the range 17.5×10^6–80×10^6 m^{-1} (e.g. Risius *et al.* 2018). We may choose $R_{unit} = 8 \times 10^7$ m^{-1}. If we take the displacement thickness to be $\delta_d^* = 1$ mm, then (2.4) indicates that

$$\delta^* \approx 0.125 \text{ mm}, \tag{2.5}$$

which leads us to take $R = 10^4$ as a typical Reynolds number. It follows from (2.2) that

$$h = 100\bar{h}. \tag{2.6}$$

The double-boundary-layer model may be viewed as the simplest model of the combustion chamber of a scramjet engine. Similar geometric configurations of various size were employed in a number of experiments to model scramjet engines. For example, Suraweera, Mee & Stalker (2005) used a chamber test section with height 60 mm to study thrust performance of a hydrogen-fuelled combustion with different inlet designs, while Lin *et al.* (2010) carried out experiments in a rectangular channel with height 131 mm to investigate supersonic mixing. Seleznev *et al.* (2019) summarised experimental data on modelling scramjets, and it was found that the height of these models varies from 30 mm to 130 mm. On noting (2.5), the corresponding non-dimensionalised distance h is estimated as

$$h = h^*/\delta^* \in (240, 1040), \tag{2.7}$$

and using this in (2.6), we obtain the range of $\bar{h}$ as $\bar{h} \in (2.4, 10.4)$, which is $O(1)$. Therefore, the present analysis is pertinent to practical realisation.

3. Twin boundary layers

As is shown in Part 1, a supersonic mode propagating in a boundary layer radiates a highly directional sound wave in the form of a Mach wave beam. Naturally, the same mathematical framework will be used here to study the coupling of the two boundary layers via the spontaneously radiated Mach waves. Formally, in the non-parallel equilibrium critical-layer regime, the near field of the radiated sound is described by the scaled

variables

$$\bar{x} = R^{-1/2}x, \quad \bar{y} = R^{-1/2}y. \tag{3.1a,b}$$

Suppose that free radiating modes with amplitude $A^{\pm}(\bar{x})$ are present in the boundary layers over the upper and lower plates. In the near field, the Mach wave radiated by the instability mode in the lower boundary layer is given by (6.9) in Part 1, and can be written as

$$p^- = \epsilon \mathscr{C}_\infty^- A^- (\bar{x} - \chi \bar{y}^-) \exp(-\mathrm{i}\alpha q y^-)\, E, \tag{3.2}$$

where $\epsilon = O(R^{-11/12})$, and $\mathscr{C}_\infty^-$ and $q = \sqrt{M^2(1-c)^2 - 1}$ are given by (4.4) in Part 1; here, $E = \exp(\mathrm{i}\alpha(x - ct))$, with α and c remaining as the streamwise wavenumber and phase velocity, respectively, and we have put $\chi = [M^2(1-c) - 1]/q$. As $\bar{y}^- \to \bar{h}$, the radiated sound acts as an impinging wave on the upper boundary layer, and has the form

$$p^- \to \epsilon \mathscr{C}_\infty^- A^- (\bar{x} - \chi \bar{h}) \exp(-\mathrm{i}\alpha q h) \exp(\mathrm{i}\alpha q y^+)\, E \equiv \epsilon R^{-1/2} p_I^+ \exp(\mathrm{i}\alpha q y^+)\, E. \tag{3.3}$$

Similarly, the Mach wave radiated by the upper boundary layer is

$$p^+ = \epsilon \mathscr{C}_\infty^+ A^+ (\bar{x} - \chi \bar{y}^+) \exp(-\mathrm{i}\alpha q y^+)\, E, \tag{3.4}$$

and as $\bar{y}^+ \to \bar{h}$,

$$p^+ \to \epsilon \mathscr{C}_\infty^+ A^+ (\bar{x} - \chi \bar{h}) \exp(-\mathrm{i}\alpha q h) \exp(\mathrm{i}\alpha q y^-)\, E \equiv \epsilon R^{-1/2} p_I^- \exp(\mathrm{i}\alpha q y^-)\, E. \tag{3.5}$$

The magnitude of the equivalent incident waves upon the upper/lower boundary layer is

$$p_I^\pm = R^{1/2} \mathscr{C}_\infty^\mp A^\mp (\bar{x} - \chi \bar{h}) \exp(-\mathrm{i}\alpha q h), \tag{3.6}$$

use of which in (4.61) of Part 1 leads to two coupled amplitude equations for $A^\pm$:

$$\left. \begin{aligned} A^{+\prime}(\bar{x}) &= \sigma \bar{x} A^+ + l A^+ |A^+|^2 + R^{1/2} \mathscr{C}_F A^- (\bar{x} - \chi \bar{h}), \\ A^{-\prime}(\bar{x}) &= \sigma \bar{x} A^- + l A^- |A^-|^2 + R^{1/2} \mathscr{C}_F A^+ (\bar{x} - \chi \bar{h}), \end{aligned} \right\} \tag{3.7}$$

where

$$\mathscr{C}_F = 2\alpha^2 q \mathscr{C}_\infty^+ \mathscr{C}_\infty^- \exp(-\mathrm{i}\alpha q h)/[c(1-c)^2 G]. \tag{3.8}$$

A notable feature is that the acoustic feedback contributes a linear term with delay to each equation, thereby coupling the dynamics of the instability modes in the two boundary layers.

If non-equilibrium effects are taken into account, then the amplitude equations are constructed by the composite theory as given by (5.10) in Part 1, and the resulting coupled system can be written as

$$\left. \begin{aligned} A^{+\prime}(\bar{x}) &= \sigma \bar{x} A^+ + \Upsilon R^{2/3} \int_0^\infty \int_0^\infty K(\xi, \eta; \bar{s})\, A^+ (\bar{x} - c\xi)\, A^+ (\bar{x} - c\xi - c\eta) \\ &\quad \times A^{+*}(\bar{x} - 2c\xi - c\eta)\, \mathrm{d}\eta\, \mathrm{d}\xi + R^{1/2} \mathscr{C}_F A^- (\bar{x} - \chi \bar{h}), \\ A^{-\prime}(\bar{x}) &= \sigma \bar{x} A^- + \Upsilon R^{2/3} \int_0^\infty \int_0^\infty K(\xi, \eta; \bar{s})\, A^- (\bar{x} - c\xi)\, A^- (\bar{x} - c\xi - c\eta) \\ &\quad \times A^{-*}(\bar{x} - 2c\xi - c\eta)\, \mathrm{d}\eta\, \mathrm{d}\xi + R^{1/2} \mathscr{C}_F A^+ (\bar{x} - \chi \bar{h}). \end{aligned} \right\} \tag{3.9}$$

Here, we restrict ourselves to the case where the upper and lower boundary layers have identical neutral radiating modes, that is, the wavenumber α and phase speed c of the
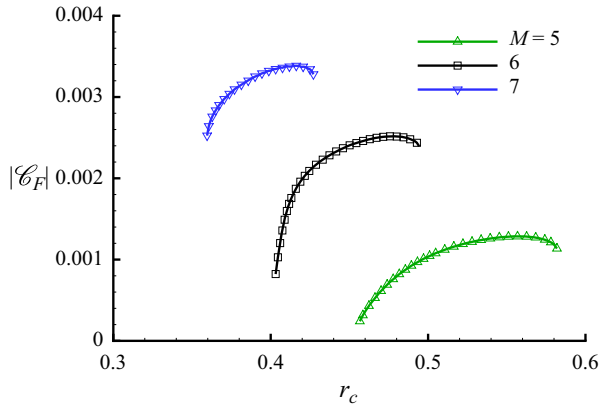
985 A14-6

Figure 2. The coefficient $\mathscr{C}_F$ versus r_c for fixed Mach numbers.

two modes are the same, hence $\sigma^+ = \sigma^- \equiv \sigma$ and $\mathscr{C}_\infty^+ = \mathscr{C}_\infty^- \equiv \mathscr{C}_\infty$. The twin boundary layers are effectively coupled. However, if the two radiating modes have different α and c, then the coupling would be through a somewhat different process.

The coefficient $\mathscr{C}_F$ measures the importance of the feedback effect, thus we evaluate its dependence on the base-flow condition. Figure 2 shows the variation of the coefficient $\mathscr{C}_F$ with the cooling ratio r_c, defined as the ratio of the wall temperature to the adiabatic wall temperature, for fixed Mach numbers $M = 5$, 6 and 7. In each case, the cooling ratio is varied in the full range where a radiating mode exists, and the magnitude of $\mathscr{C}_F$ is approximately $O(10^{-3})$. Since typical Reynolds numbers are of $O(10^4)$, the effect of the feedback term is not negligible if $\bar{h}$ is not too large.

As $\bar{x} \to -\infty$, the instability modes take the linear form

$$A^\pm(\bar{x}) = a_0^\pm \exp(\sigma \bar{x}^2/2) + \cdots, \tag{3.10}$$

where $a_0^\pm$ is an arbitrary constant representing the initial amplitude. In order to achieve the right balance of the terms in the amplitude equation (3.9), we need that

$$R^{1/2} |\mathscr{C}_F| |A^\pm(\bar{x} - \chi \bar{h})| = O(|\sigma|) \quad \text{for } \bar{x} = O(1), \tag{3.11}$$

which is possible when $\bar{h} \gg 1$. Since $|\bar{x} - \chi \bar{h}| \gg 1$, we may use (3.10) to estimate the feedback term as

$$R^{1/2} |\mathscr{C}_F| |a_0^\pm| \exp(\sigma_r(\bar{x} - \chi \bar{h})^2/2) = R^{1/2} |\mathscr{C}_F| |a_0^\pm| \exp(\sigma_r[\chi^2 \bar{h}^2 + \bar{x}(\bar{x} - 2\chi \bar{h})]/2)$$
$$= O(|\sigma|), \tag{3.12}$$

which implies

$$\bar{h} = O\left(\chi^{-1}\sqrt{2\ln(R^{-1/2} |\mathscr{C}_F|^{-1} |\sigma|)/\sigma_r}\right) \gg 1. \tag{3.13}$$

Note that the feedback term is of $O(1)$ only when $\bar{x}(\bar{x} - 2\chi \bar{h}) = O(1)$, i.e. $|\bar{x}| = O(1/\bar{h})$; outside this region, the feedback is smaller for $\bar{x} < 0$, while the feedback is much greater for $\bar{x} > 0$.

In the limit of $\bar{h}$ being larger than assumed by (3.13), that is,

$$\bar{h} \gg \bar{h}_c \equiv \chi^{-1}\sqrt{2\ln(R^{-1/2}\,|\mathscr{C}_F|^{-1}\,|\sigma|)/\sigma_r}, \tag{3.14}$$

$p_I^{\pm} \to 0$ for $\bar{x} \ll \chi\bar{h} - \sqrt{2\ln(R^{-1/2}\,|\mathscr{C}_F|^{-1}\,|\sigma|)/\sigma_r}$, that is, the feedback effect diminishes. The feedback effect kicks in when $\bar{x} > \chi\bar{h} - \sqrt{2\ln(R^{-1/2}\,|\mathscr{C}_F|^{-1}\,|\sigma|)/\sigma_r}$, and specifically, when $\bar{x} - \chi\bar{h} = O(1)$, the feedback term is a factor of $R^{1/2}\,|\mathscr{C}_F|$ greater than other terms in the amplitude equation (3.9) no matter how large $\bar{h}$ is. However, for the near-field solution of the sound radiation to be applicable, we require $\bar{h} \ll R^{1/2}$. When $\bar{h} = O(R^{1/2})$, the far-field solution must be used, in which case the local growth rate A' depends on A at downstream positions (Wu 2005).

On noting that $|\mathscr{C}_F| = O(10^{-3})$ and $|\sigma| = O(10^{-1})$ for the present $M = 6$ boundary layer with a $T_w = 3$ isothermal surface, and that a typical Reynolds number is taken as $R = 10^4$, we have $|\mathscr{C}_F| > R^{-1/2}\,|\sigma|$, and the coefficient of the feedback term, $R^{1/2}\,|\mathscr{C}_F|$, is found to be $O(10^{-1})$, suggesting that the feedback effect is likely to be significant. For other flows that involve coupling via feedback mechanisms, the magnitude of the coefficient $\mathscr{C}_F$ may be greater; these scenarios are evaluated in § 3.3.

With the nonlinear terms ignored but the feedback terms accounted for, the initial condition for the coupled equations (3.9) is derived as

$$A^{\pm}(\bar{x}) = a_0^{\pm}\exp(\sigma\bar{x}^2/2) - \frac{R^{1/2}\mathscr{C}_F}{\sigma\chi\bar{h}}a_0^{\mp}\exp(\sigma(\bar{x}-\chi\bar{h})^2/2), \tag{3.15}$$

where use has been made of (3.10). It follows that even if the two base-flow boundary layers are identical, the amplitudes of the modes can be different in general since they are dependent on the initial amplitude $a_0^{\pm}$. We may have two symmetric solutions with $A^+ = A^- \equiv A$ and $a_0^+ = a_0^- \equiv a_0$, in which case the two amplitude equations (3.9) reduce to a single one,

$$A'(\bar{x}) = \sigma\bar{x}A + \Upsilon R^{2/3}\int_0^{\infty}\int_0^{\infty}K(\xi,\eta;\bar{s})\,A(\bar{x}-c\xi)\,A(\bar{x}-c\xi-c\eta)$$
$$\times A^*(\bar{x}-2c\xi-c\eta)\,\mathrm{d}\eta\,\mathrm{d}\xi + R^{1/2}\mathscr{C}_F A(\bar{x}-\chi\bar{h}), \tag{3.16}$$

with the initial condition (3.15) becoming

$$A(\bar{x}) = a_0\left[\exp(\sigma\bar{x}^2/2) - \frac{R^{1/2}\mathscr{C}_F}{\sigma\chi\bar{h}}\exp(\sigma(\bar{x}-\chi\bar{h})^2/2)\right] \quad \text{as } \bar{x} \to -\infty. \tag{3.17}$$

Likewise, we may also have two antisymmetric solutions with $A^+ = -A^- \equiv A$ and $a_0^+ = -a_0^- \equiv a_0$. Then the governing equations (3.9) become

$$A'(\bar{x}) = \sigma\bar{x}A + \Upsilon R^{2/3}\int_0^{\infty}\int_0^{\infty}K(\xi,\eta;\bar{s})\,A(\bar{x}-c\xi)\,A(\bar{x}-c\xi-c\eta)$$
$$\times A^*(\bar{x}-2c\xi-c\eta)\,\mathrm{d}\eta\,\mathrm{d}\xi - R^{1/2}\mathscr{C}_F A(\bar{x}-\chi\bar{h}), \tag{3.18}$$

with the initial condition

$$A(\bar{x}) = a_0\left[\exp(\sigma\bar{x}^2/2) + \frac{R^{1/2}\mathscr{C}_F}{\sigma\chi\bar{h}}\exp(\sigma(\bar{x}-\chi\bar{h})^2/2)\right] \quad \text{as } \bar{x} \to -\infty. \tag{3.19}$$

More generally, we can introduce the gauge transformation $A^- = A^+\,\mathrm{e}^{\mathrm{i}\phi}$, where ϕ is a parameter. It can be shown that the two amplitude equations (3.9) reduce to two equations

that are consistent only if $e^{i\phi} = e^{-i\phi}$, i.e. $e^{i\phi} = \pm 1$, implying that the above two cases are the only possibilities for reducing the two equations into one.

3.1. *Symmetric and antisymmetric cases*

The amplitude equations pertinent to the symmetric and antisymmetric cases are now studied in some detail. Nonlinearity may not be important in the amplitude equation if the initial amplitude a_0 is sufficiently small (e.g. $a_0 = 1$), in which case we can study the linearised versions of (3.16) and (3.18). Take (3.16) as an example. Neglecting the nonlinear term leads to the linear feedback equation

$$A'(\bar{x}) = \sigma \bar{x} A + R^{1/2} \mathscr{C}_F A(\bar{x} - \chi \bar{h}). \tag{3.20}$$

Equation (3.20) subject to the initial condition (3.17) can be solved analytically. Taking the Fourier transform of (3.20), we obtain

$$ik\hat{A} = i\sigma \hat{A}' + R^{1/2} \mathscr{C}_F \exp(-ik\chi \bar{h}) \hat{A}, \tag{3.21}$$

where $\hat{A}$ is the transformed function of the variable k. Equation (3.21) is solved to give

$$\hat{A}(k) = A_0 \exp \left\{ \frac{1}{\sigma} \left(\frac{k^2}{2} - \frac{R^{1/2} \mathscr{C}_F}{\chi \bar{h}} \exp(-ik\chi \bar{h}) \right) \right\}, \tag{3.22}$$

where A_0 is a constant to be fixed by the initial condition (3.17). On applying the Fourier inverse formula, the solution for $A(\bar{x})$ is found as

$$A(\bar{x}) = \frac{A_0}{2\pi} \int_{-\infty}^{\infty} \exp \left\{ \frac{1}{\sigma} \left(\frac{k^2}{2} - \frac{R^{1/2} \mathscr{C}_F}{\chi \bar{h}} \exp(-ik\chi \bar{h}) \right) + ik\bar{x} \right\} \mathrm{d}k. \tag{3.23}$$

To determine A_0, let us first consider the case of no feedback, i.e. equation $A'(\bar{x}) = \sigma \bar{x} A$ subject to the initial condition $A(\bar{x}) = a_0 \exp(\sigma \bar{x}^2/2)$ as $\bar{x} \to -\infty$. The solution is a Gaussian, $A(\bar{x}) = a_0 \exp(\sigma \bar{x}^2/2)$. On the other hand, by a formula similar to (3.23), we have

$$A(\bar{x}) = \frac{A_0}{2\pi} \int_{-\infty}^{\infty} \exp(k^2/(2\sigma) + ik\bar{x}) \, \mathrm{d}k = A_0 \sqrt{\frac{|\sigma|}{2\pi}} \exp(i(\pi - \psi)/2) \exp(\sigma \bar{x}^2/2), \tag{3.24}$$

where ψ is the phase of $1/2\sigma$ defined in $[\pi/2, 3\pi/2]$. By equating the above solution to $A(\bar{x}) = a_0 \exp(\sigma \bar{x}^2/2)$, the constant A_0 is found as

$$A_0 = \sqrt{2\pi/|\sigma|} \exp(-i(\pi - \psi)/2) \, a_0. \tag{3.25}$$

Thus the solution to (3.20) subject to the initial condition (3.17) can be written as

$$A(\bar{x}) = a_0 \frac{\exp(-i(\pi - \psi)/2)}{\sqrt{2\pi |\sigma|}} \int_{-\infty}^{\infty} \exp \left\{ \frac{1}{\sigma} \left(\frac{k^2}{2} - \frac{R^{1/2} \mathscr{C}_F}{\chi \bar{h}} \exp(-ik\chi \bar{h}) \right) + ik\bar{x} \right\} \mathrm{d}k. \tag{3.26}$$

The ensuing calculations will be carried out for the same base-flow condition as given in Part 1, a $M = 6$ boundary layer with a $\bar{T}_w = 3$ isothermal surface ($r_c = 0.427$). As a first step, we compare the analytical solution (3.26) with the numerical solution to the linear feedback equation (3.20). The numerical approach is the sixth-order
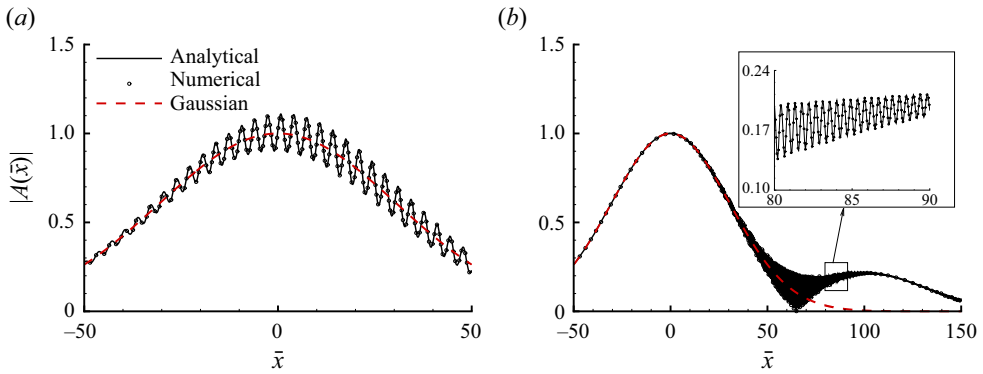
Figure 3. Comparison between the analytical solution (3.26) and the numerical solution to (3.20) with (a) $a_0 = 1$ for $\bar{h} = 2$, and (b) $\bar{h} = 15$ with an enlarged feedback coefficient $\mathscr{C}_F = 3 \times 10^{-2}$.
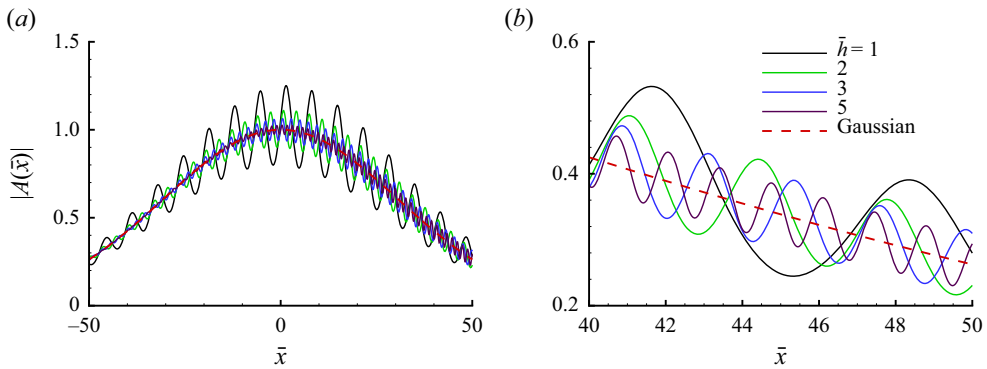

Figure 4. (a) Effects of $\bar{h}$ on the solution to the linear feedback equation (3.20) with $a_0 = 1$. (b) Zoom-in to the range $40 < \bar{x} < 50$ in (a).

Adams–Moulton method. Figure 3 depicts the two solutions in a wide range of $\bar{x}$, showing that the two solutions overlap each other. Different from the Gaussian distribution when the feedback is absent, the solution in the presence of the feedback exhibits highly oscillatory behaviour, which is due to the double exponential in the Fourier integral as is given by (3.26). Moreover, in the case of the enlarged feedback coefficient $\mathscr{C}_F$, the solution undergoes near extinction followed by resurrection (figure 3b).

Figure 4 shows the effect of $\bar{h}$, which measures the distance between the two plates, on the linear evolution of the mode. For moderate values of $\bar{h}$ (1 and 2), the oscillations are significant in both the upstream and downstream regions. As $\bar{h}$ increases, the feedback effect is not obvious in the upstream region, but kicks in later in the downstream region. It is expected that the linear modal evolution with feedback reduces to the case of no reflection (represented by a Gaussian distribution) as $\bar{h} \to \infty$. This is confirmed by the comparison in figure 5, which indicates that the solutions with $\bar{h} = 50$ and 20 overlap with the Gaussian in a fairly large range. However, the feedback effect will still appear eventually in the region further downstream due to the finite value of $\bar{h}$, but that region is not relevant to the present theory. Figure 5(b) shows that the solution with $\bar{h} = 10$ oscillates about the Gaussian in the downstream region, indicating that the feedback effect remains in action, albeit being much reduced.
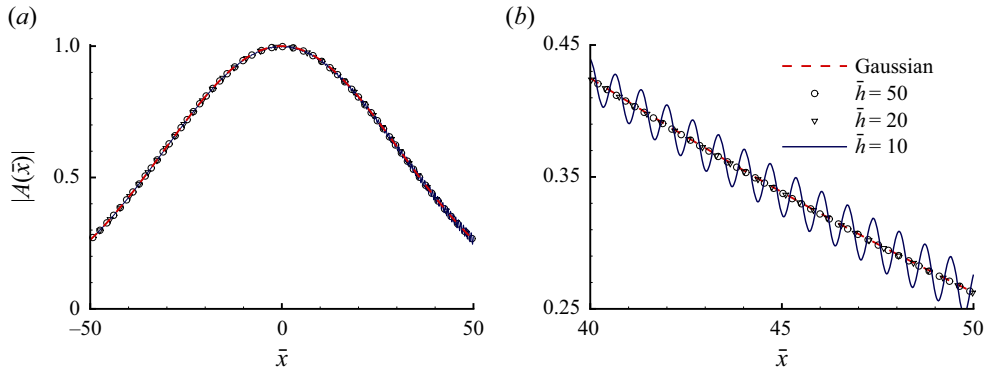
985 A14-10

Figure 5. (*a*) The solution to the linear feedback equation (3.20) with $a_0 = 1$ and comparison with that for large values of $\bar{h}$ as well as the case of no reflection. (*b*) Zoom-in to the range $40 < \bar{x} < 50$ in (*a*).
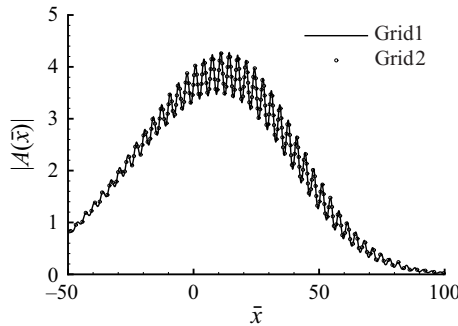

Figure 6. Resolution check on the solution to the nonlinear feedback equation (3.16) with $a_0 = 3$ and $\bar{h} = 2$. The step size of 'Grid2' is half of that of 'Grid1'.

The nonlinear feedback equation (3.16) is solved numerically for a moderate value of $\bar{h}$, and the results are shown in figure 6, where two grid sizes are employed to ensure satisfactory accuracy.

To see how nonlinearity affects the solutions with feedback, we fix $\bar{h} = 2$ and vary the initial amplitude a_0 when solving the linear and nonlinear feedback equations (3.20) and (3.16). These results are displayed in figure 7. As expected, there is little difference between the linear and nonlinear solutions for $a_0 = 1$ (figure 7*a*). As the magnitude of a_0 increases, nonlinear effects are no longer negligible. For $a_0 = 3$, the nonlinear and linear solutions are qualitatively similar but there is appreciable quantitative difference, with the amplitude acquiring a larger value under the influence of nonlinearity (figure 7*b*). For $a_0 = 3.65$, a qualitative difference is observed: the nonlinear solution develops a singularity at a finite distance, $\bar{x}_s$ say, while the linear counterpart attenuates, and so does the nonlinear one without feedback (figure 7*c*). Dictated by the nonlinear term, the singularity is of the form (Leib 1991),

$$A \rightarrow a_\infty (\bar{x}_s - \bar{x})^{-(5/2 + \mathrm{i}\phi_s)} \quad \text{as } \bar{x} \rightarrow \bar{x}_s, \tag{3.27}$$

where ϕ_s and a_∞ are constants. Increasing further the initial amplitude to $a_0 = 5$, the nonlinear solutions with and without feedback both blow up, with the former exhibiting oscillations, whereas the linear solution still undergoes highly oscillatory attenuation (figure 7*d*).
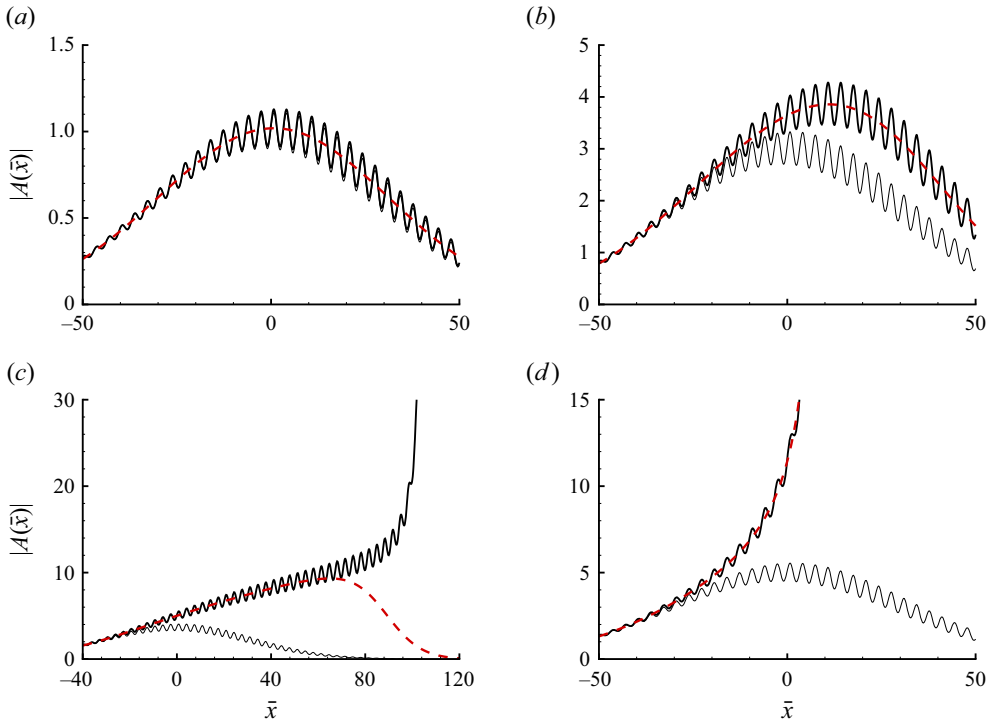
Figure 7. Effects of the initial amplitude a_0 on the solution to the nonlinear feedback equation (3.16) with $\bar{h} = 2$, for (*a*) $a_0 = 1$, (*b*) $a_0 = 3$, (*c*) $a_0 = 3.65$, (*d*) $a_0 = 5$. Thick solid lines indicate solution to (3.16); thin solid lines indicate solution to (3.20); dashed lines indicate nonlinear solution without feedback.

Next, we evaluate the effects of $\bar{h}$ on the nonlinear solution with feedback. Figure 8(*a*) shows that when $a_0 = 3$, the solutions for all five non-zero $\bar{h}$ are bounded. The feedback causes rapid oscillations. For large values of $\bar{h}$ (e.g. 5), the feedback effect is not obvious in the upstream region, but becomes significant later in the downstream region. As $\bar{h}$ is reduced, the feedback effect becomes significant in both the upstream and downstream regions, causing oscillations about the solution without reflection (figure 8*b*). Increasing further the magnitude of a_0, the solutions for various values of $\bar{h}$ all terminate at a finite-distance singularity but in an oscillatory manner, as is shown in figures 8(*c*,*d*).

For the antisymmetric case with small initial amplitude, the solution to the linear feedback equation

$$A'(\bar{x}) = \sigma \bar{x} A - R^{1/2} \mathscr{C}_F A(\bar{x} - \chi \bar{h}), \tag{3.28}$$

together with the initial condition (3.19), can be obtained numerically, or evaluated using the analytical solution, which corresponds to (3.26) with the sign in the second term in the exponent being changed to positive. The effects of $\bar{h}$ on the linear and nonlinear solutions turn out to be, by and large, similar to those of the symmetric case, hence they are not presented.

3.2. *The coupled equations*

We now consider the system of the coupled equations (3.9), taking the case of $\bar{h} = 2$ for illustration. For each fixed total amplitude

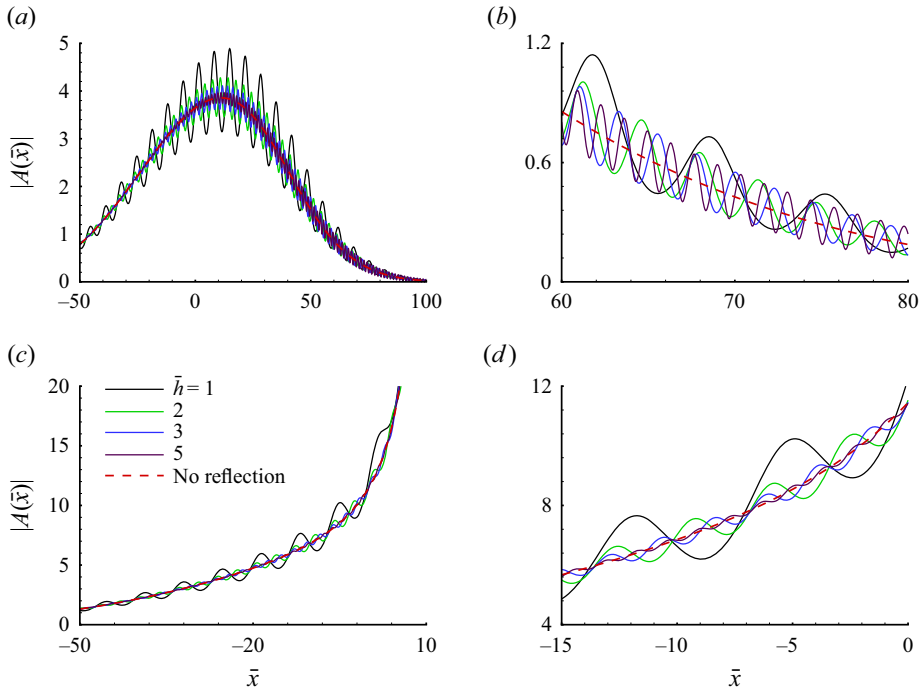$$\check{a}_0 \equiv \sqrt{(a_0^+)^2 + (a_0^-)^2}, \tag{3.29}$$

Figure 8. Effects of $\bar{h}$ on the solution to the nonlinear feedback equation (3.16) for (*a*) $a_0 = 3$ and (*c*) $a_0 = 5$. (*b*,*d*) Zoom-in plots for the ranges $60 < \bar{x} < 80$ and $-15 < \bar{x} < 0$ in (*a*,*c*), respectively.

we vary the amplitude ratio a_0^+/a_0^-. Figure 9 shows the evolution of the coupled modes with different initial amplitude ratios for $\check{a}_0 = 1$, which is sufficiently small that nonlinearity is unimportant in the entire course of the development. Figure 9(*a*) depicts the evolution of the two modes for $a_0^+/a_0^- = 0$. In this case, mode A^+, initially unseeded, is excited by mode A^- through the Mach wave radiated by the latter. Mode A^+ starts to grow downstream even though in the upstream region its amplitude is rather small. Due to the nature of coupling, mode A^+ also reaches a peak at a downstream position, and in turn affects the evolution of mode A^-, resulting in small oscillations of its amplitude in the downstream region. The development of the coupled modes for the case $a_0^+/a_0^- = 0.3$ is shown in figure 9(*b*). The amplitudes of both modes, A^+ and A^-, attenuate in the downstream region after attaining their respective maxima. Mode A^- grows first and is followed by decay with minor oscillations, while mode A^+ exhibits strong oscillations due to the impact of the stronger mode A^+. When $a_0^+/a_0^- = 0.7$, both modes A^+ and A^- experience notable oscillations as they evolve downstream (figure 9*c*). Figure 10 shows the evolution of the coupled modes in the case $\check{a}_0 = 3.6$, for which nonlinearity becomes important but does not cause blow-up yet. The trend of the evolution is similar to the case $\check{a}_0 = 1$, that is, the feedback effect, manifested as oscillations, becomes more appreciable as the amplitude ratio increases. Another feature is that the envelope of the mode is strongly distorted due to nonlinearity (figures 10*a*,*b*). In all three cases, the solutions indicate that the nonlinear interaction and coupling cause vigorous energy exchange between the two modes. The development of the coupled modes with different initial amplitude ratios for $\check{a}_0 = 5$ is shown in figure 11. When $a_0^+/a_0^- = 0$ (figure 11*a*), mode A^- rapidly develops a singularity at a finite distance while also exciting mode A^+, which
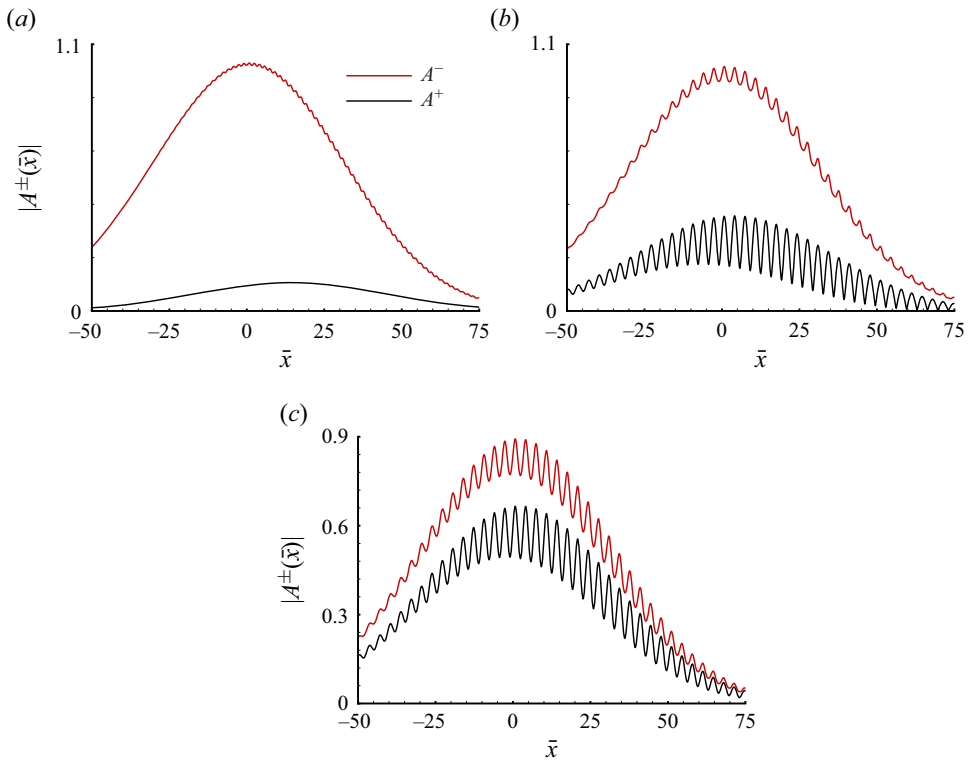
Figure 9. Effects of the amplitude ratio on the solution to the coupled equations (3.9) with $\bar{h} = 2$ and $\sqrt{(a_0^+)^2 + (a_0^-)^2} = 1$, for (a) $a_0^+/a_0^- = 0$, (b) $a_0^+/a_0^- = 0.3$, (c) $a_0^+/a_0^- = 0.7$.

blows up subsequently. It is interesting to note that the singularities of two modes are of the same form as (3.27) but do not appear simultaneously. Moreover, oscillations are hardly appreciable, indicating that in this case, nonlinearity becomes dominant; mode A^- already terminates at a singularity before mode A^+ acquires an amplitude large enough to act back on A^-. As the amplitude ratio increases, oscillations develop on the amplitudes of both modes and become stronger before a finite-distance singularity occurs (figures 11b,c).

3.3. *Evolution with large values of $\mathscr{C}_F$*

The amplitude equation (3.9) describing the coupling of the radiating modes in two supersonic boundary layers through acoustic feedback is in fact generic, and may arise in other types of flows. For example, the effective coupling may take place in two supersonic planar or circular jets, since each also radiates highly directional Mach waves (Tam 1995; Wu 2005). While the magnitude of the coefficient $\mathscr{C}_F$ measuring the effect of coupling in the present twin boundary layer is $O(10^{-3})$ and rather moderate, it could be much larger in other flows, e.g. twin jets, since the radiation turned out to be stronger (Wu 2005). In view of this, we study the the amplitude equation with feedback for artificially increased $\mathscr{C}_F$.

By fixing $\mathscr{C}_F = 3 \times 10^{-2}$ and keeping other parameters unchanged, we perform a numerical study of (3.16). With typical Reynolds number remaining as $R = 10^4$, the magnitude of the coefficient of the feedback term, $R^{1/2}|\mathscr{C}_F|$, is found to be $O(1)$. Figure 12 shows the solution to (3.16) for different $\bar{h}$. For $a_0 = 3$, the feedback effect is
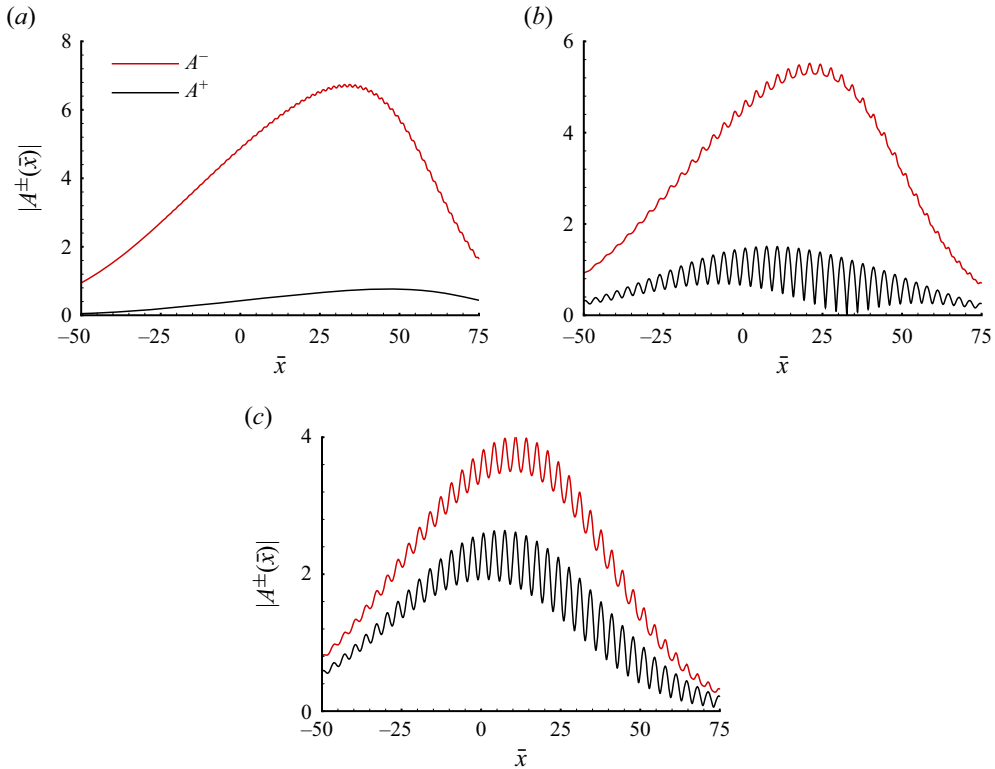
985 A14-14

Figure 10. Effects of the amplitude ratio on the solution to the coupled equations (3.9) with $\bar{h} = 2$ and $\sqrt{(a_0^+)^2 + (a_0^-)^2} = 3.6$, for (a) $a_0^+/a_0^- = 0$, (b) $a_0^+/a_0^- = 0.3$, (c) $a_0^+/a_0^- = 0.7$.

significant even for $\bar{h}$ as large as 15, causing the amplitude to undergo strong and rapid oscillations (figures 12a,b). A notably different feature is that with a larger $\bar{h}$, e.g. $\bar{h} = 15$, the envelope of the amplitude attenuates to an almost diminished level and then resurrects. This resurgence is due to the enlarged feedback effect, by which the emitted sound wave re-excites the mode, at a later time due to substantial delay. For $a_0 = 5$ (figures 12c,d), the solutions for different $\bar{h}$ all blow up, with oscillations resembling those in the case of moderate $|\mathscr{C}_F|$ (cf. figures 8c,d).

4. Cousin boundary layers

We now consider the case where the upper plate has a different surface temperature. A band of radiating modes may still exist on each boundary layer, but the nearly neutral modes do not have the same frequency and wavelength. In this case, for a radiating mode on the lower boundary layer, the upper boundary layer acts as a pure reflector with a finite reflection. We refer to these two boundary layers as 'cousin boundary layers', a configuration that is more general than the twin boundary layers, and more representative of practical applications. The distance between the two plates is still chosen as $h = O(R^{1/2})$ so that the upper and lower boundary layers share a common acoustic near field in the core. The reflection process is again described by the Cartesian coordinates $(x, y^+)/(x, y^-)$ for the upper/lower plate, as shown in figure 1.
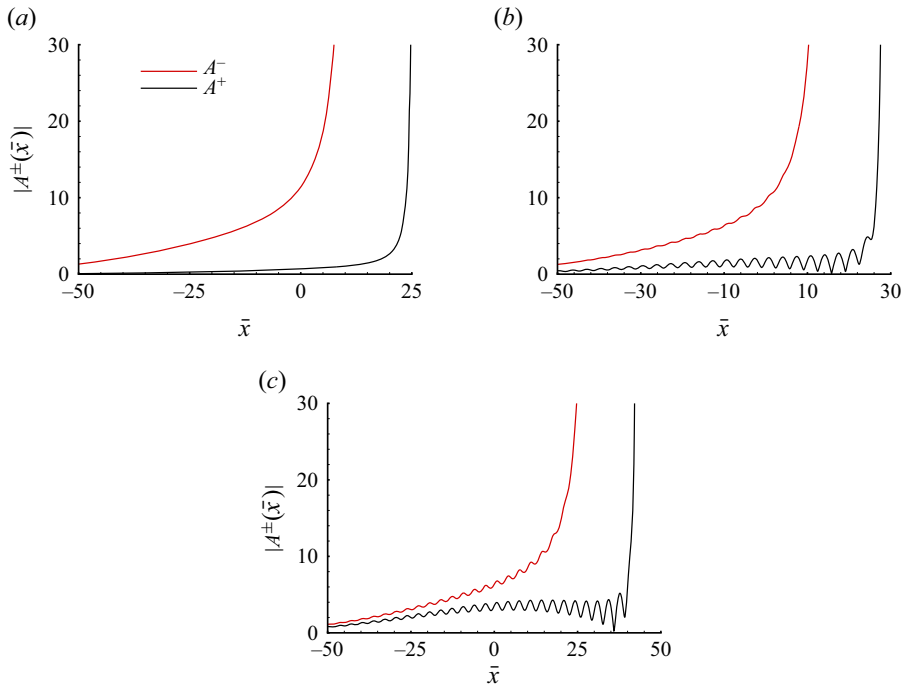
Figure 11. Effects of the amplitude ratio on the solution to the coupled equations (3.9) with $\bar{h} = 2$ and $\sqrt{(a_0^+)^2 + (a_0^-)^2} = 5$, for (a) $a_0^+/a_0^- = 0$, (b) $a_0^+/a_0^- = 0.3$, (c) $a_0^+/a_0^- = 0.7$.

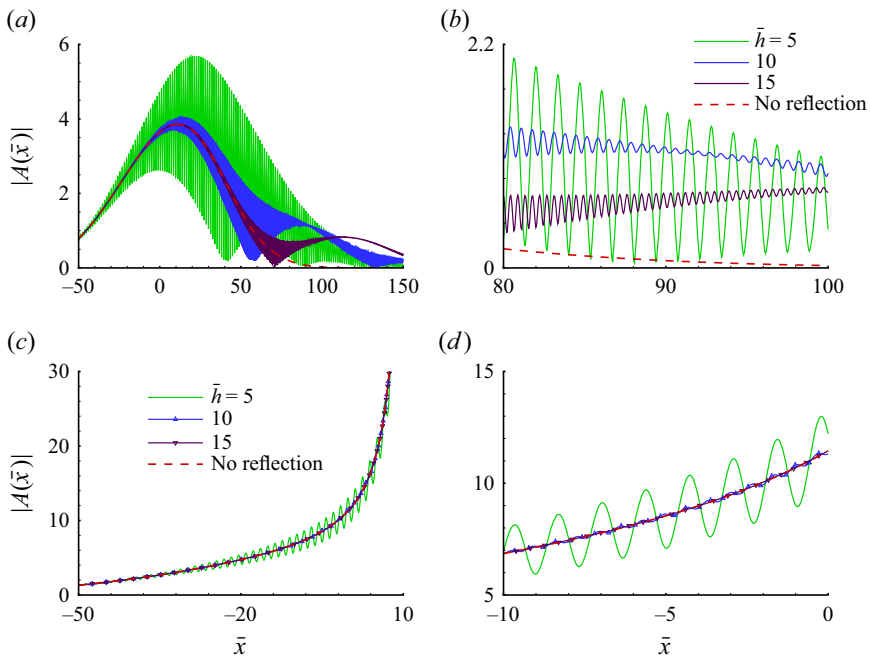Figure 12. Effects of $\bar{h}$ on the solution to the nonlinear feedback equation (3.16) for (a) $a_0 = 3$ and (c) $a_0 = 5$, with $\mathscr{C}_F = 3 \times 10^{-2}$. (b,d) Zoom-in plots for the ranges $80 < \bar{x} < 100$ and $-10 < \bar{x} < 0$ in (a,c), respectively.

The near-field Mach wave radiated from the lower boundary layer is given by (6.9) in Part 1, and can be written as (3.2), and setting $y^- = \bar{h}$ in this gives the incident sound wave upon the upper boundary layer:

$$p^- \to \epsilon \mathscr{C}_\infty A(\bar{x} - \chi \bar{h}) \exp(-\mathrm{i}\alpha q h) \exp(\mathrm{i}\alpha q y^+) E \equiv \epsilon R^{-1/2} p_I^+ \exp(\mathrm{i}\alpha q y^+) E, \quad (4.1)$$

where we have put

$$p_I^+(\bar{x}) = R^{1/2} \mathscr{C}_\infty A(\bar{x} - \chi \bar{h}) \exp(-\mathrm{i}\alpha q h). \quad (4.2)$$

The radiated Mach wave is reflected back to the lower boundary layer to act as an incident wave. The reflection process is similar to that considered in Part 1, and is described briefly here. In the main upper boundary layer, the disturbance has the expansion

$$\begin{aligned}
(\rho^+, u^+, v^+, p^+, \theta^+) &= \epsilon R^{-1/2} (\hat{\rho}_0^+, \hat{u}_0^+, \hat{v}_0^+, \hat{p}_0^+, \hat{\theta}_0^+)(\bar{x}, y^+) E \\
&\quad + \epsilon R^{-1} (\hat{\rho}_1^+, \hat{u}_1^+, \hat{v}_1^+, \hat{p}_1^+, \hat{\theta}_1^+) + \mathrm{c.c.} + \cdots. \quad (4.3)
\end{aligned}$$

Substitution of the above expansion into (2.2) in Part 1 followed by linearisation and elimination of $\hat{\rho}_0^+$, $\hat{u}_0^+$, $\hat{v}_0^+$ and $\hat{\theta}_0^+$ yields at leading order the Rayleigh equation for the pressure, $\mathscr{L}\hat{p}_0^+ = 0$, where the operator $\mathscr{L}$ is defined by (2.29) in Part 1. As $y^+ \to \infty$,

$$\hat{p}_0^+ \sim p_I^+(\bar{x}) \left[\exp(\mathrm{i}\alpha q y^+) + \mathscr{R} \exp(-\mathrm{i}\alpha q y^+) \right], \quad (4.4)$$

where the reflection coefficient $\mathscr{R}$ is determined by performing a linear critical-layer analysis together with numerical integration as described in Part 1. At the next order, a routine calculation shows that the pressure $\hat{p}_1^+$ satisfies an inhomogeneous Rayleigh equation

$$\mathscr{L}\hat{p}_1^+ = \frac{2\mathrm{i}c}{\alpha} \left\{ \frac{\bar{U}'}{(\bar{U}-c)^2} \frac{\partial^2 \hat{p}_0^+}{\partial \bar{x} \partial y^+} + \frac{\alpha^2}{c} \left[\frac{M^2 \bar{U}(\bar{U}-c)}{\bar{T}} - 1 \right] \frac{\partial \hat{p}_0^+}{\partial \bar{x}} \right\} - \bar{x}\Delta^+, \quad (4.5)$$

where

$$\begin{aligned}
\Delta^+ &= \left\{ \frac{2\bar{U}'}{\bar{U}-c} \left(\frac{\bar{U}_1}{\bar{U}-c} - \frac{\bar{U}_1'}{\bar{U}'} \right) + \frac{\bar{T}'}{\bar{T}} \left(\frac{\bar{T}_1'}{\bar{T}'} - \frac{\bar{T}_1}{\bar{T}} \right) \right\} \frac{\partial \hat{p}_0^+}{\partial y^+} \\
&\quad + \alpha^2 M^2 \frac{(\bar{U}-c)^2}{\bar{T}} \left(\frac{2\bar{U}_1}{\bar{U}-c} - \frac{\bar{T}_1}{\bar{T}} \right) \hat{p}_0^+. \quad (4.6)
\end{aligned}$$

As $y^+ \to \infty$,

$$\begin{aligned}
\hat{p}_1^+ &\sim \hat{p}_I(\bar{x}) [\exp(\mathrm{i}\alpha q y^+) + \hat{\mathscr{R}}(\bar{x}) \exp(-\mathrm{i}\alpha q y^+)] \\
&\quad + q^{-1}[M^2(1-c) - 1] p_I^{+\prime}(\bar{x}) y^+ (\exp(\mathrm{i}\alpha q y^+) - \mathscr{R} \exp(-\mathrm{i}\alpha q y^+)). \quad (4.7)
\end{aligned}$$

Evidently, the main-layer expansion breaks down when $y^+ = O(R^{1/2})$, thus we introduce $\bar{y}^+ = R^{-1/2} y^+$ corresponding to the common acoustic region. The perturbation

now expands as

$$(\rho^+, u^+, v^+, p^+, \theta^+) = \epsilon R^{-1/2}(\rho_0^+, u_0^+, v_0^+, p_0^+, \theta_0^+)$$
$$+ \epsilon R^{-1}(\rho_1^+, u_1^+, v_1^+, p_1^+, \theta_1^+) + \cdots. \quad (4.8)$$

At leading order, the pressure p_0^+ satisfies the wave equation $\mathcal{L}_w p_0^+ = 0$, with the operator $\mathcal{L}_w$ being given by (6.1) in Part 1. The solution takes the form

$$p_0^+ = \check{p}_\mathcal{I}(\bar{x}, \bar{y}^+) \exp(i\alpha(x - ct + qy^+)) + \check{p}_\mathcal{R}(\bar{x}, \bar{y}^+) \exp(i\alpha(x - ct - qy^+)) + \text{c.c.}, \quad (4.9)$$

where $\check{p}_\mathcal{I}$ and $\check{p}_\mathcal{R}$ are to be determined by considering the second-order term p_1^+, which is governed by the equation

$$\mathcal{L}_w p_1^+ = 2\left[\frac{\partial^2 p_0^+}{\partial \bar{x} \partial x} + \frac{\partial^2 p_0^+}{\partial \bar{y}^+ \partial y^+} - M^2 \left(\frac{\partial}{\partial t} + \frac{\partial}{\partial x} \right) \frac{\partial p_0^+}{\partial \bar{x}} \right]. \quad (4.10)$$

To remove the secular terms in the expansion, we must require that the term proportional to p_0^+ on the right-hand side of the above equation be zero. Moreover, matching with the main-layer solution leads to

$$\left. \begin{aligned} [M^2(1 - c) - 1]\frac{\partial \check{p}_\mathcal{I}}{\partial \bar{x}} - q \frac{\partial \check{p}_\mathcal{I}}{\partial \bar{y}^+} &= 0, \\ \check{p}_\mathcal{I}(\bar{x}, \bar{y}^+) = p_I^+(\bar{x}) \quad \text{at } \bar{y}^+ = 0, \end{aligned} \right\} \quad (4.11)$$

and

$$\left. \begin{aligned} [M^2(1 - c) - 1]\frac{\partial \check{p}_\mathcal{R}}{\partial \bar{x}} + q \frac{\partial \check{p}_\mathcal{R}}{\partial \bar{y}^+} &= 0, \\ \check{p}_\mathcal{R}(\bar{x}, \bar{y}^+) = \mathcal{R} p_I^+(\bar{x}) \quad \text{at } \bar{y}^+ = 0. \end{aligned} \right\} \quad (4.12)$$

The solution to (4.11) is $\check{p}_\mathcal{I}(\bar{x}, \bar{y}^+) = p_I^+(\bar{x} + \chi \bar{y}^+)$, which is the radiated wave from the lower boundary layer since

$$\epsilon R^{-1/2} \check{p}_\mathcal{I}(\bar{x}, \bar{y}^+) \exp(i\alpha(x - ct + qy^+))$$
$$= \epsilon \mathcal{C}_\infty A(\bar{x} + \chi \bar{y}^+ - \chi \bar{h}) \exp(-i\alpha qh) \exp(i\alpha qy^+) E$$
$$= \epsilon \mathcal{C}_\infty A(\bar{x} - \chi \bar{y}^-) \exp(-i\alpha qy^-) E = \epsilon p_0^-, \quad (4.13)$$

which is exactly (3.2). The solution to (4.12) is $\check{p}_\mathcal{R}(\bar{x}, \bar{y}^+) = \mathcal{R} p_I^+(\bar{x} - \chi \bar{y}^+)$. This solution represents the outgoing wave for the upper boundary layer, and serves as the incident wave for the lower boundary layer. We can write

$$p_\mathcal{R}^+ \equiv \epsilon R^{-1/2} \check{p}_\mathcal{R}(\bar{x}, \bar{y}^+) \exp(i\alpha(x - ct - qy^+))$$
$$= \epsilon \mathcal{R} \mathcal{C}_\infty A(\bar{x} - \chi \bar{y}^+ - \chi \bar{h}) \exp(-i\alpha qh) \exp(-i\alpha qy^+) E$$
$$= \epsilon \mathcal{R} \mathcal{C}_\infty A(\bar{x} - \chi \bar{y}^+ - \chi \bar{h}) \exp(-2i\alpha qh) \exp(i\alpha qy^-) E. \quad (4.14)$$

As $\bar{y}^+ \to \bar{h}$, the reflected wave by the upper boundary layer has the form

$$p_\mathcal{R}^+ \to \epsilon \mathcal{R} \mathcal{C}_\infty A(\bar{x} - 2\chi \bar{h}) \exp(-2i\alpha qh) \exp(i\alpha qy^-) E \equiv \epsilon R^{-1/2} p_I^-(\bar{x}) \exp(i\alpha qy^-) E, \quad (4.15)$$

where we have put

$$p_I^-(\bar{x}) = R^{1/2} \mathscr{R} \mathscr{C}_\infty A(\bar{x} - 2\chi\bar{h}) \exp(-2\mathrm{i}\alpha q h). \tag{4.16}$$

Substitution of the above expression into the amplitude equation (4.61) and use of the composite amplitude equation (5.10) in Part 1 leads to

$$A'(\bar{x}) = \sigma\bar{x}A + \Upsilon R^{2/3} \int_0^\infty \int_0^\infty K(\xi, \eta; \bar{s}) A(\bar{x} - c\xi) A(\bar{x} - c\xi - c\eta)$$

$$\times A^*(\bar{x} - 2c\xi - c\eta) \, \mathrm{d}\eta \, \mathrm{d}\xi + R^{1/2} \mathscr{C}_R \mathscr{R} A(\bar{x} - 2\chi\bar{h}), \tag{4.17}$$

where

$$\mathscr{C}_R = 2\alpha^2 q \mathscr{C}_\infty^2 \exp(-2\mathrm{i}\alpha q h)/[c(1-c)^2 G], \tag{4.18}$$

comparison of which with (3.8) shows that $|\mathscr{C}_R| = |\mathscr{C}_F|$. Similar to the twin boundary layers, the acoustic feedback contributes a linear term with delay (which is twice as long). The initial condition is found as

$$A(\bar{x}) = a_0 \left[\exp(\sigma\bar{x}^2/2) - \frac{R^{1/2} \mathscr{C}_R \mathscr{R}}{2\sigma\chi\bar{h}} \exp(\sigma(\bar{x} - 2\chi\bar{h})^2/2) \right] \quad \text{as } \bar{x} \to -\infty. \tag{4.19}$$

Since the coefficient $\mathscr{C}_R \mathscr{R}$ in the amplitude equation (4.17) measures the importance of the reflection-facilitated feedback effect, we first evaluate its dependence on the base-flow parameters. Figures 13(a,c,e) show the variation of $\mathscr{C}_R \mathscr{R}$ with the upper wall temperature T_w^+ for several values of fixed lower wall temperature T_w^- at different Mach numbers. In each case, the coefficient $\mathscr{C}_R \mathscr{R}$ remains more or less constant and small (being of $O(10^{-3})$), but increases rapidly when approaching the resonant temperature ($T_w^+ = T_w^-$), at which point $\mathscr{C}_R \mathscr{R}$ becomes infinite. Figures 13(b,d,f) show the variation of $\mathscr{C}_R \mathscr{R}$ with the lower wall cooling ratio r_c^- for fixed upper wall temperature T_w^+ at Mach numbers $M = 5$, 6 and 7. In each case, r_c^- is varied in the full range where a radiating mode exists. There is no significant difference of $\mathscr{C}_R \mathscr{R}$ for various T_w^+ except for T_w^+ that is in the range of the existence of the radiating mode, e.g. $T_w^+ = 2.5$, 3 and 3.5 for $M = 5$, 6 and 7, respectively. For such values of T_w^+, $\mathscr{C}_R \mathscr{R}$ raises quickly in a narrow range of r_c^-, which contains $T_w^+ = T_w^-$, at which resonance takes place and correspondingly $\mathscr{C}_R \mathscr{R}$ becomes unbounded.

4.1. *Effects of upper wall temperature*

We first calculate the reflection coefficient $\mathscr{R}$ for different upper wall temperatures T_w^+ with a given Mach number $M = 6$ and fixed lower wall temperature $T_w^- = 3$. The magnitude of the reflection coefficient turns out to be almost unity for most upper wall temperatures, except that it increases rapidly when the wall temperature corresponding to the resonant case ($T_w^+ = T_w^- = 3$) is approached. Using these results, we perform a numerical study of the amplitude equation (4.17) for different T_w^+ with $M = 6$ and $T_w^- = 3$. Three representative initial amplitudes are considered: $a_0 = 3$, for which nonlinearity just becomes appreciable, $a_0 = 3.6$, for which nonlinearity becomes significant but the solution remains bounded (and finally attenuates), and $a_0 = 5$, in which case the solution blows up. Figures 14(a,b) show that for the two moderate values of a_0 (3 and 3.6), the acoustic feedback induces oscillations to the amplitude of the supersonic mode, similar to the case of a twin boundary layer even though the feedback is now facilitated through the reflected Mach wave emitted by the same boundary layer. The amplitude evolution
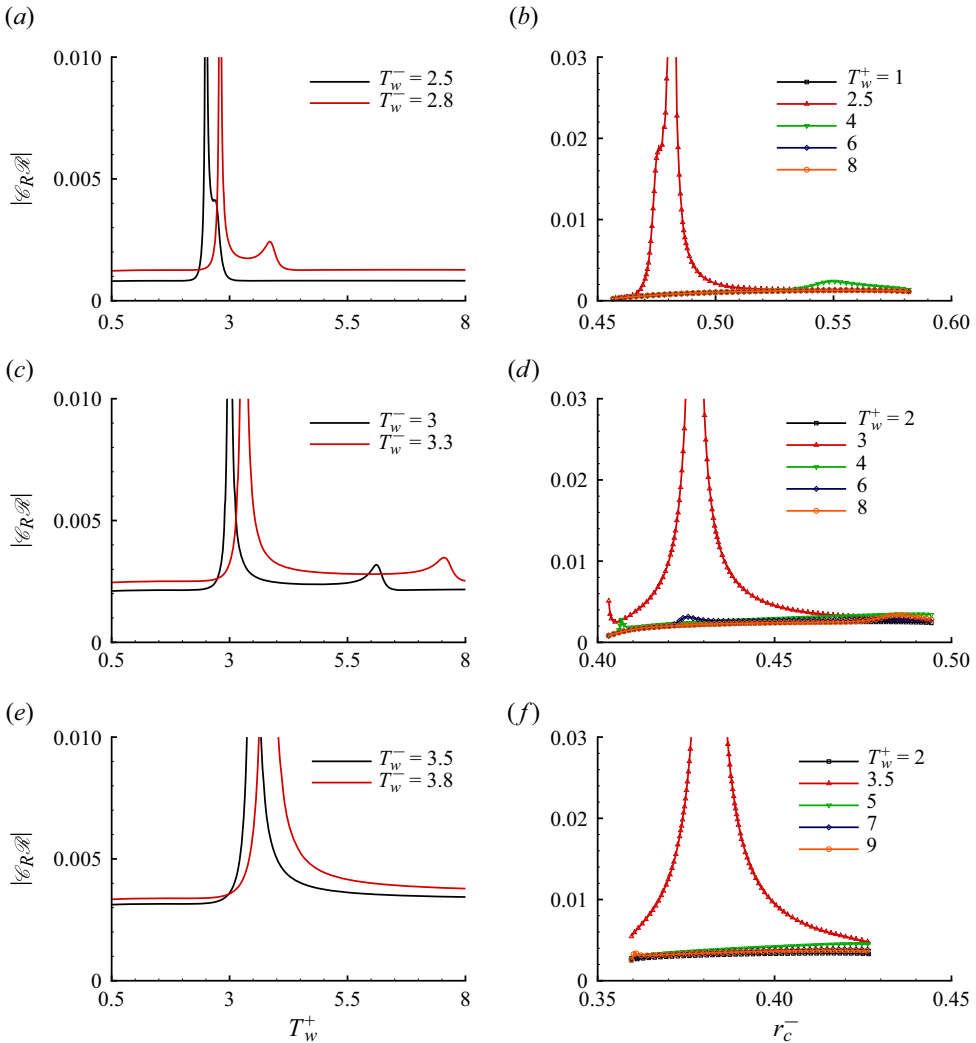
Figure 13. The coefficient $\mathscr{C}_R\mathscr{R}$ versus (a,c,e) the upper wall temperature T_w^+ and (b,d,f) the lower wall cooling ratio r_c^-, for Mach numbers (a,b) $M = 5$, (c,d) $M = 6$ and (e,f) $M = 7$. The ranges of the existence of the radiating mode are $r_c^- \in [0.457, 0.582]$ ($T_w^- \in [2.37, 3.02]$), $r_c^- \in [0.403, 0.494]$ ($T_w^- \in [2.83, 3.47]$) and $r_c^- \in [0.36, 0.427]$ ($T_w^- \in [3.3, 3.92]$) for $M = 5$, 6 and 7, respectively.

appears much the same for various T_w^+, with small differences being just visible in the enlarged views. With initial amplitude $a_0 = 5$ (figure 14c), the solutions all blow up, with the feedback effect manifested as barely appreciable oscillations, and the effect of T_w^+ on the evolution is also negligible.

Figure 15 shows the nonlinear evolution of the radiating mode in the lower boundary layer when the upper and lower wall temperatures are close ($T_w^+ \approx T_w^- = 3$). Figure 15(a) compares the modal evolution for different T_w^+ with $a_0 = 3$, where nonlinearity is moderate. It is seen that the mode amplitude for different T_w^+ oscillates about the solution without reflection. As T_w^+ approaches T_w^- (i.e. nearly satisfies the resonant condition), the oscillations become more intense due to the rapid increase of the reflection coefficient. This is also true for $a_0 = 3.6$, for which the nonlinear effect becomes enhanced but
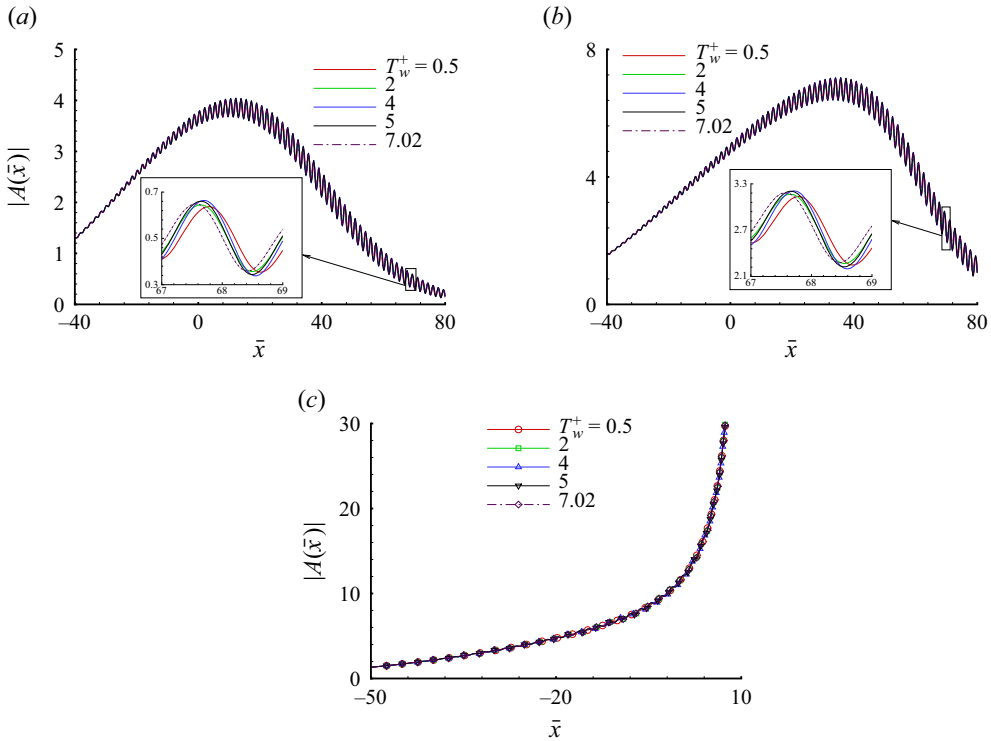
985 A14-20

Figure 14. Effects of the upper wall temperature T_w^+ on the solution to the amplitude equation (4.17) with $\bar{h} = 2$, for (*a*) $a_0 = 3$, (*b*) $a_0 = 3.6$, (*c*) $a_0 = 5$. Here, $T_w^+ = 7.02$ corresponds to the adiabatic wall condition. The lower wall temperature is $T_w^- = 3$, and the Mach number is $M = 6$.

without causing a finite-distance singularity (figure 15*b*). When $a_0 = 5$ (figure 15*c*), all the solutions blow up in an oscillatory manner, with oscillations becoming more pronounced closer to the resonant condition. The present theory ceases to be applicable when the temperatures of the two walls are extremely close, and instead needs to be reformulated as a 'detuned' twin-boundary-layer model.

While much attention has been paid to linear radiating modes, whose radiating characteristics have been fairly well understood, back effects of the radiated sound on their linear and nonlinear evolution have not been studied previously. There exist no experimental or computational data with which our theoretical predictions could be compared. Nevertheless, we noted, upon completion of the present work, that recently Chen, Wang & Fu (2021) employed the method of linear parabolised stability equations to trace the development of radiating modes in a hypersonic boundary layer over a wedge. They found that the amplitude underwent considerable oscillations (see e.g. figure 15(*c*) in the paper), despite the facts that no rigid reflecting surface was present and that a monotonic amplification or decay was predicted by linear stability theory. This puzzling outcome was attributed to the beating effect of multiple coexisting modes, which may be amplifying or damped. An alternative but more plausible explanation, based on the main finding of the present work, could be that the shock, which is present in their problem, acts to reflect the spontaneously radiated sound, thereby establishing an acoustic back action akin to what was studied here. Our assertion is also based upon the realisation that an amplitude equation of the same form as (4.17) can be derived in the case of reflection by
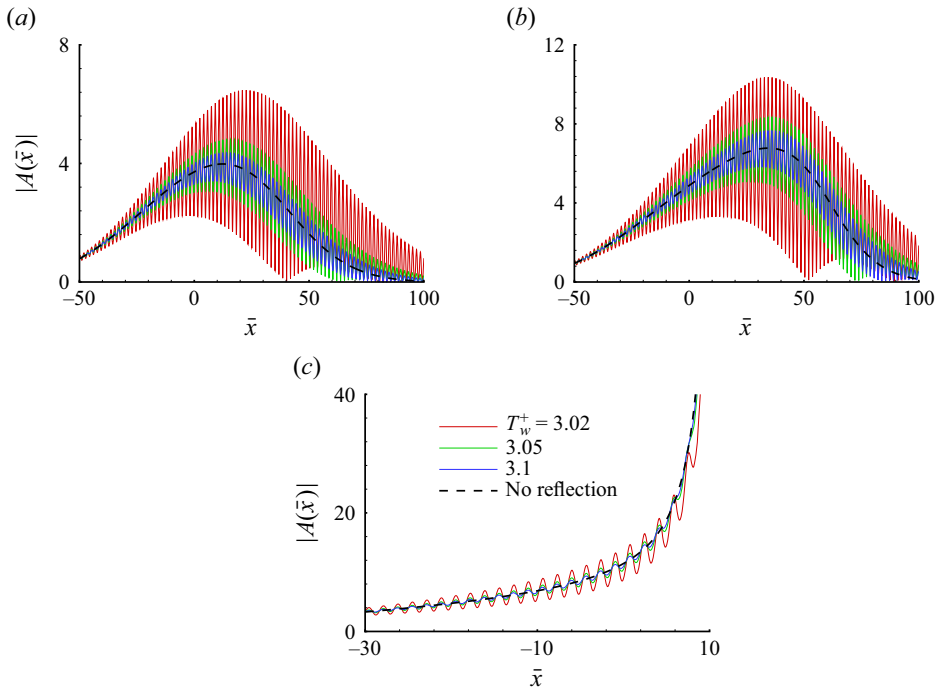
985 A14-21

Figure 15. Strong oscillations of the solution to the amplitude equation (4.17) with $\bar{h} = 2$ when the upper wall temperature T_w^+ approaches the lower wall temperature $T_w^- = 3$, for (a) $a_0 = 3$, (b) $a_0 = 3.6$, (c) $a_0 = 5$. The Mach number is $M = 6$.

a shock. It is worth noting that an imperfect non-reflecting far-field boundary condition in numerical calculations could also cause similar behaviour, which would of course be an artefact. This implies that for numerical methods to capture faithfully and accurately the radiating mode and its evolution, it is important to specify an appropriate far-field condition. Numerical simulations to validate the theoretical findings would be a major undertaking and are deemed beyond the scope of the present study. We hope that our theoretical work would prompt computational and experimental studies.

4.2. *Evolution with large values of $\mathscr{C}_R$*

Again, the magnitude of the coefficient $\mathscr{C}_R$ representing the effect of coupling may be larger in certain types of flows, e.g. a supersonic jet adjacent to a reflecting surface, which mimics a jet engine installed on a wing (Cavalieri *et al.* 2014; Lyu *et al.* 2017). An amplitude equation similar to (4.17) can be derived, but stronger Mach wave radiation could lead to a greater $\mathscr{C}_R$. With this perspective in mind, we now solve the amplitude equation (4.17) for an artificially increased $\mathscr{C}_R$, i.e. $\mathscr{C}_R = 3 \times 10^{-2}$. We now take a somewhat large $\bar{h} = 7$, for which the feedback effect may be significant, as will be seen, and keep other parameters unchanged. Figure 16 shows the effects of T_w^+ on the nonlinear evolution of the radiating mode in the lower boundary layer. For $a_0 = 3$ and 3.6, the results are displayed in figures 16(*a,b*). In addition to the usual rapid oscillations of the amplitude, the envelope of the amplitude features a second peak in the downstream region. The resurrection after the mode is nearly extinct is again due to the enlarged feedback term in (4.17), which re-excites the radiating mode after a fairly long delay. The zoomed views
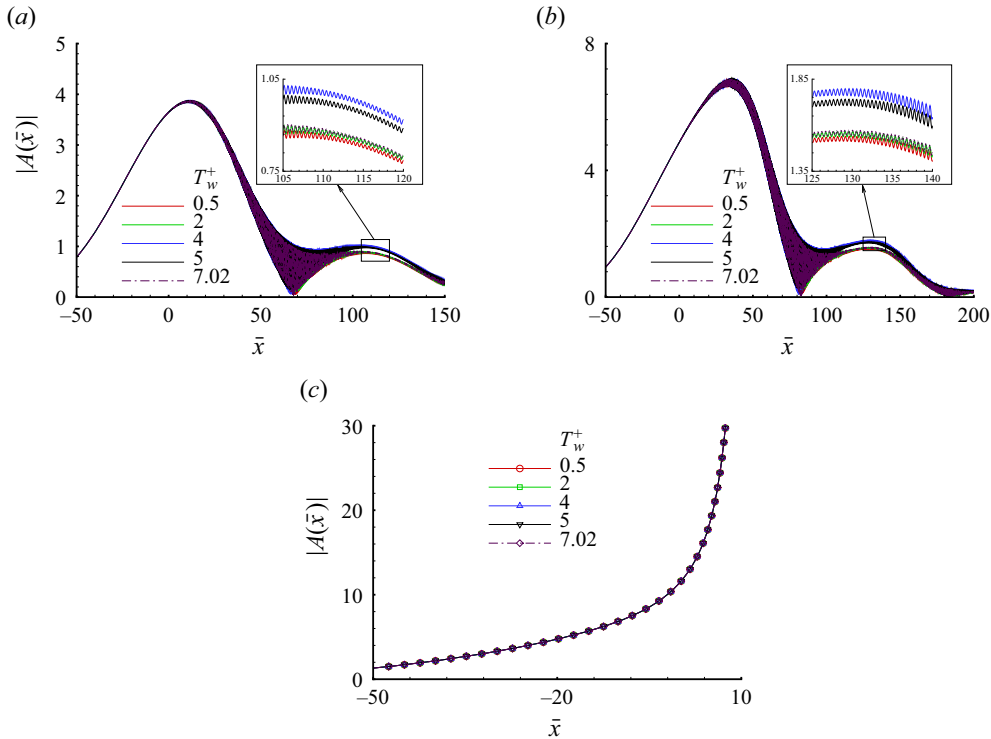
985 A14-22

Figure 16. Effects of the upper wall temperature T_w^+ on the solution to the amplitude equation (4.17) with $\bar{h} = 7$ and $\mathscr{C}_R = 3 \times 10^{-2}$, for (a) $a_0 = 3$, (b) $a_0 = 3.6$, (c) $a_0 = 5$. Here, $T_w^+ = 7.02$ corresponds to the adiabatic wall condition. The lower wall temperature is $T_w^- = 3$, and the Mach number is $M = 6$.

in figures 16(a,b) indicate that strong cooling (e.g. $T_w^+ = 0.5, 2$) or the adiabatic condition ($T_w^+ = 7.02$) results in a smaller second peak compared with the cases $T_w^+ = 4$ and 5, but the overall difference is barely appreciable. For the case $a_0 = 5$, the amplitude rapidly blows up within a finite distance due to the nonlinear effect, which is dominant over the acoustic feedback such that the latter plays hardly any role (figure 16c), and in this case the solution is little influenced by T_w^+.

5. Summary and conclusions

In this paper, we investigated linear and nonlinear evolution of supersonic instability modes under the back action of the Mach waves radiated spontaneously by the modes themselves. This scenario of acoustic feedback was considered in the simplest setting of two supersonic boundary layers developing along two semi-infinite parallel plates. The distance separating the two plates is assumed to be comparable with the transverse extent of the near field of the Mach waves, a configuration representative of the combustion chamber of a scramjet. Using the formula for the Mach wave radiation in the near field, the amplitude equations are derived for two cases of relevance: the twin boundary layers and cousin boundary layers.

For the so-called twin boundary layers, where the wall conditions are identical, the Mach wave radiated from the instability mode in one boundary layer impacts that in the other. This process is described by a system of coupled amplitude equations, in which the contribution of the back effects enters in the form of a linear term of delay type.

In the special cases where the modes in the two boundary layers are in symmetric and antisymmetric phases, the system reduces to a single-amplitude equation. The system of the coupled amplitude equations, including its reduced forms, was studied analytically and numerically. The evolution characteristics were found to depend on the distance between the plates, measured by the rescaled distance $\bar{h}$, as well as on the initial amplitudes of the supersonic modes and their ratio. For moderate values of $\bar{h}$, the primary effect of the acoustic feedback is to induce rapid oscillations of the modal amplitudes, which remain bounded for small or moderate initial amplitudes, but blow up (i.e. develop a singularity at finite distances) when the initial amplitudes are large enough. The feedback plays a destabilising role in general, enhancing the modal amplitude, causing singularity which is otherwise absent, and in the extreme case of a supersonic mode being seeded in only one boundary layer exciting the supersonic mode in the other. The ratio of the initial amplitudes changes the evolution significantly, and specifically renders the blow-up to occur at different downstream locations. In the limit of the rescaled plate separation $\bar{h} \to \infty$, the evolution reduces, as expected, to the case of no acoustic back effect.

In the more general case of the so-called cousin boundary layers, where the wall temperatures are different, the spontaneously emitted Mach wave by the supersonic mode in one of the boundary layers is reflected back by the other to affect the original radiating mode. The amplitude equation was derived, which consists of a linear term of delay type representing the acoustic feedback. Since the amplitude equation is rather similar to those in the case of twin boundary layers, the acoustic feedback plays a similar role, namely, causes the amplitude to oscillate rapidly. It is found that if the wall temperature is not too close to the resonant condition, then the reflection coefficient is almost a constant and hence the development of the instability mode appears the same. However, if the wall temperature is close to the resonant condition, then the reflected wave becomes stronger than the Mach wave originally emitted, resulting in greater feedback effects on the modal evolution, which manifest as strong oscillations of the modal amplitude.

The amplitude equations pertinent to twin and cousin boundary layers could arise in other situations, such as twin jets or a jet adjacent to a rigid surface, where the feedback effect may be stronger. In view of such broad applications, we also solved the amplitude equations with the coefficients of the feedback terms being increased by one order of magnitude. The acoustic feedback effect turns out to be still significant for fairly large $\bar{h}$. With longer delays of the feedback action, the amplitude of the instability mode not only exhibits rapid oscillations, but also experiences near extinction followed by resurrection, which occurs due to the sound wave emitted earlier re-exciting the supersonic mode at a later time.

The present theoretical investigation provides physical insights into how the spontaneously radiated Mach waves and the instability modes could be effectively coupled in double supersonic boundary layers. The results are deemed useful for assessing the impact of the noise emitted from the tunnel walls on the supersonic mode evolving in the boundary layer over the test model. They are probably relevant also for instability and transition in scramjet combustion chambers as well as for twin-jet engines or jet engines installed in the vicinity of a surface (wing or fuselage).

Declaration of interests. The authors report no conflict of interest.

Author ORCIDs.

Ⓘ Fufeng Qin https://orcid.org/0009-0006-3975-168X;

Ⓘ Xuesong Wu https://orcid.org/0000-0002-3406-8017.

REFERENCES

ABO, T., INASAWA, A. & ASAI, M. 2021 Experimental study on the feedback-loop mechanism generating tonal protuberance noise in boundary layers. *Eur. J. Mech. (B/Fluids)* **85**, 46–57.

ALKISLAR, M.B., KROTHAPALLI, A., CHOUTAPALLI, I. & LOURENCO, L. 2005 Structure of supersonic twin jets. *AIAA J.* **43**, 2309–2318.

ARBEY, H. & BATAILLE, J. 1983 Noise generated by aerofoil placed in a uniform laminar flow. *J. Fluid Mech.* **134**, 33–47.

BHAT, T.R.S. & BLACKNER, A.M. 1998 Installed jet noise prediction model for coaxial jets. *AIAA Paper* 98-79.

BOZAK, R. & HENDERSON, B. 2011 Aeroacoustic experiments with twin jets. *AIAA Paper* 2011-2790.

BUSHELL, K. 1975 Measurement and prediction of jet noise in flight. *AIAA Paper* 75-461.

CAVALIERI, A.V.G., JORDAN, P., WOLF, W.R. & GERVAIS, Y. 2014 Scattering of wavepackets by a flat plate in the vicinity of a turbulent jet. *J. Sound Vib.* **333**, 6516–6531.

CHEN, X., WANG, L. & FU, S. 2021 Parabolized stability analysis of hypersonic thermal–chemical nonequilibrium boundary-layer flows. *AIAA J.* **59**, 2382–2395.

CURRAN, E.T., HEISER, W.H. & PRATT, D.T. 1996 Fluid phenomena in scramjet combustion systems. *Annu. Rev. Fluid Mech.* **28**, 323–360.

DESQUESNES, G., TERRACOL, M. & SAGAUT, P. 2007 Numerical investigation of the tone noise mechanism over laminar airfoils. *J. Fluid Mech.* **591**, 155–182.

GOLUBEV, V. 2021 Recent advances in acoustics of transitional airfoils with feedback-loop interactions: a review. *Appl. Sci.* **11**, 1057.

GRAZIOSI, P. & BROWN, G. 2002 Experiments on stability and transition at Mach 3. *J. Fluid Mech.* **474**, 83–124.

JONES, L.E. & SANDBERG, R.D. 2011 Numerical analysis of tonal airfoil self-noise and acoustic feedback-loops. *J. Sound Vib.* **330**, 6137–6152.

JONES, L.E., SANDBERG, R.D. & SANDHAM, N.D. 2010 Stability and receptivity characteristics of a laminar separation bubble on an aerofoil. *J. Fluid Mech.* **648**, 257–296.

KLUWICK, A. & KORNFELD, M. 2014 Triple-deck analysis of transonic high Reynolds number flow through slender channels. *Phil. Trans. R. Soc. Lond.* **372**, 20130346.

KUO, C.-W., CLUTS, J. & SAMIMY, M. 2017 Exploring physics and control of twin supersonic circular jets. *AIAA J.* **55**, 68–85.

LAUFER, J. 1961 Aerodynamic noise in supersonic wind tunnels. *J. Aerosp. Sci.* **28**, 685–692.

LEIB, S.J. 1991 Nonlinear evolution of subsonic and supersonic disturbances on a compressible free shear layer. *J. Fluid Mech.* **224**, 551–578.

LIN, K.C., RYAN, M., CARTER, C., GRUBER, M. & RAFFOUL, C. 2010 Raman scattering measurements of gaseous ethylene jets in a Mach 2 supersonic crossflow. *J. Propul. Power* **26**, 503–513.

LYU, B. & DOWLING, A.P. 2018 Experimental validation of the hybrid scattering model of installed jet noise. *Phys. Fluids* **30**, 085102.

LYU, B., DOWLING, A.P. & NAQAVI, I. 2017 Prediction of installed jet noise. *J. Fluid Mech.* **811**, 234–268.

MOORE, A. 2004 A 3D prediction of the wing reflection of aero engine noise. *AIAA Paper* 2004-2865.

PATERSON, R.W., VOGT, P.G., FINK, M.R. & MUNCH, C.L. 1973 Vortex noise of isolated airfoils. *J. Aircraft* **10**, 296–302.

QIN, F. & WU, X. 2024 Excitation and evolution of radiating modes in supersonic boundary layers. Part 1. Fundamental resonance with impinging sound waves. *J. Fluid Mech.* **985**, A13.

RAMAN, G., PANICKAR, P. & CHELLIAH, K. 2012 Aeroacoustics of twin supersonic jets: a review. *Intl J. Aeroacoust.* **11**, 957–984.

RISIUS, S., COSTANTINI, M., KOCH, S., HEIN, S. & KLEIN, C. 2018 Unit Reynolds number, Mach number and pressure gradient effects on laminar–turbulent transition in two-dimensional boundary layers. *Exp. Fluids* **59**, 1–29.

ROCKWELL, D. & NAUDASHER, E. 1979 Self-sustained oscillations of impinging free shear layers. *Annu. Rev. Fluid Mech.* **11**, 67–94.

SCHNEIDER, S.P. 2001 Effect of high-speed tunnel noise on laminar–turbulent transition. *J. Spacecr. Rockets* **38**, 323–333.

SELEZNEV, R.K., SURZHIKOV, S.T. & SHANG, J.S. 2019 A review of the scramjet experimental data base. *Prog. Aerosp. Sci.* **106**, 43–70.

SMITH, F.T. 1989 On the first-mode instability in subsonic, supersonic or hypersonic boundary layers. *J. Fluid Mech.* **198**, 127–153.

SMITH, F.T. & BODONYI, R.J. 1980 On the stability of the developing flow in a channel or circular pipe. *Q. J. Mech. Appl. Maths* **33**, 293–320.

SURAWEERA, M., MEE, D. & STALKER, R. 2005 Skin friction reduction in hypersonic turbulent flow by boundary layer combustion. *AIAA Paper* 2005-613.

TAM, C.K.W. 1995 Supersonic jet noise. *Annu. Rev. Fluid Mech.* **27**, 17–43.

WAY, D. & TURNER, B. 1980 Model tests demonstrating under-wing installation effects on engine exhaust noise. *AIAA Paper* 80-1048.

WU, X. 2005 Mach wave radiation of nonlinearly evolving supersonic instability modes in shear layers. *J. Fluid Mech.* **523**, 121–159.

WU, X. 2011 On generation of sound in wall-bounded shear flows: back action of sound and global acoustic coupling. *J. Fluid Mech.* **689**, 279–316.

WU, X. 2014 On the role of acoustic feedback in boundary-layer instability. *Phil. Trans. R. Soc. Lond.* **372**, 20130347.